ACS Sustainable Chemistry & Engineering

Research Article

Cite This: ACS Sustainable Chem. Eng. 2019, 7, 2316−2326

pubs.acs.org/journal/ascecg

The Hydration of β- and α'_H-Dicalcium Silicates: An X-ray Spectromicroscopic Study

Jiaqi Li,[†] Guoqing Geng,*[,†,‡] Wenxin Zhang,[†] Young-Sang Yu,[§] David A. Shapiro,[§] and Paulo J. M. Monteiro[†]

[†]Department of Civil and Environmental Engineering, University of California, Berkeley, 725 Davis Hall, Berkeley, California 94720, United States

[‡]Laboratory for Waste Management, OHLD/004, Paul Scherrer Institut, 5232 Villigen PSI, Switzerland

[§]Advanced Light Source, Lawrence Berkeley National Laboratory, Building 2, 0437, Berkeley, California 94720, United States

Supporting Information

ABSTRACT: Dicalcium silicate (C_2S) is an important clinker mineral in Portland and belite-calcium sulfoaluminate cement. However, there is still a lack of information on the local degree of silicate polymerization and calcium coordination in C_2S hydration products. This study aimed to fill this gap by characterizing the hydration of two C_2S polymorphs, the β- and α'_H- types, using scanning transmission X-ray microscopy coupled with ptychographic imaging. The results showed that the coordination of the Ca species in β- and α'_H-C_2S had a distorted, cubic-like symmetry, whereas the Ca coordination of calcium silicate hydrate (C-S-H), the main hydration product, was structurally similar to that of tobermorite. The outer hydration product (Op) of both polymorphs exhibited an increasing degree of silicate polymerization over time. The inner hydration product (Ip) of β-C_2S polymerized slower than Op; however, the degree of silicate polymerization of both Ip and Op in the α'_H-C_2S hydration system was comparable. The polymerization degree of Op was relatively heterogeneous, whereas, in α'_H-C_2S, the polymerization degree was more homogeneous. Ptychographic imaging shows that the Op of α'_H-C_2S exhibits coarser fibrils than the Op of β-C_2S, and a clear Op−Ip interface of hydrated β-C_2S is observed.

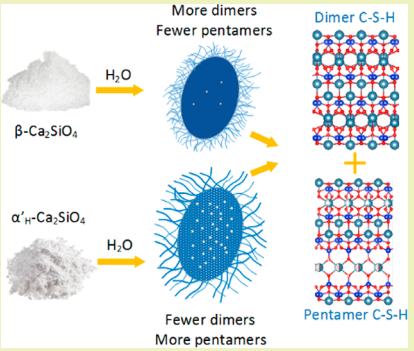

KEYWORDS: *Portland cement, Dicalcium silicate, Low carbon cement, Silicate chain polymerization, Calcium silicate hydrate, Calcium coordination, Morphology*

INTRODUCTION

Concrete is the second most consumed material after water.[1] Its strength comes from the hydration of cement. The production of conventional Portland cement (PC) accounts for 8−9% of global CO_2 emission and 2−3% of energy consumption.[2] The major compounds of PC clinker are tricalcium silicate (Ca_3SiO_5, also termed C_3S in cement chemistry notation), dicalcium silicate (Ca_2SiO_4, also termed C_2S; or belite as impure C_2S), tricalcium aluminate ($Ca_3Al_2O_6$), and tetracalcium aluminoferrite (Ca_2AlFeO_5). Among them, C_3S is the most abundant phase, but it has the highest environmental impact due to the high calcination temperatures and heavy CO_2 emission from decomposing limestone. The cement industry is under increasing pressure to reduce CO_2 emissions and energy consumption. Production of C_2S-rich PC at the expense of the typically more abundant C_3S is one way to lower the environmental impact of PC manufacturing.[3] For example, belite-calcium sulfoaluminate (BCSA) cement is a very promising alternative to PC because the calcination temperature of BCSA is 200 °C lower than PC.[4] BCSA cement (also belite-rich) manufacturing is capable of reducing CO_2 emission and energy consumption by 30% and 20%, respectively.[5]

The main binding phase of hardened PC pastes and concretes is a calcium silicate hydrate (C-S-H) gel. The structure and properties of C-S-H govern the mechanical properties and durability of PC-based materials.[6,7] The well-accepted molecular models of C-S-H (Figure 1) are created by modifying a tobermorite structure[8] with defected dreierkette-type silicate chains, which are composed of bridging and pairing tetrahedra, flanked on CaO_7 sheets to form the calcium silicate basal layer. The neighboring basal layers are separated by zeolitic calcium ions and water.[9] The structures of synthetic nanocrystalline C-S-Hs have been extensively studied at the atomic, molecular, and nano scales. However, the atomic and molecular structures (e.g., Ca and Si coordination) of hydration product C-S-H have been inadequately studied due to their poor ordering along the *c*-axis. Understanding the

Received: October 2, 2018
Revised: November 18, 2018
Published: December 20, 2018

DOI: 10.1021/acssuschemeng.8b05060
ACS Sustainable Chem. Eng. 2019, 7, 2316−2326

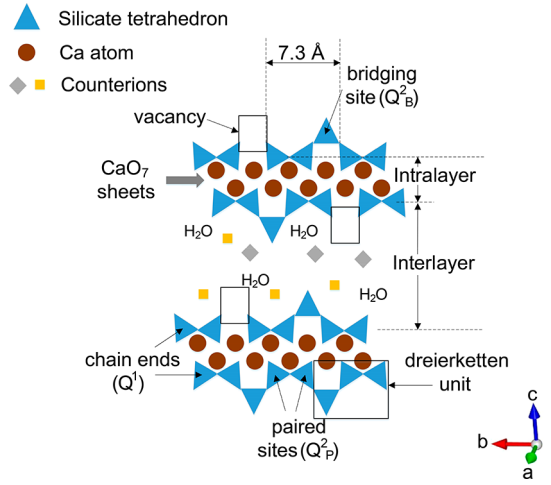

Figure 1. Schematic representation of the nanostructures of C-S-H. The brown circles represent Ca species in the Ca-O sheet, and blue triangles are silicate units in paired and bridging sites. The gray diamonds and yellow squares represent sites which can be occupied by cations that charge-neutralize the structure as a whole (e.g., Ca^{2+} and/or K^+).

structure and properties of C-S-H is essential for optimizing the properties of sustainable cement-based materials.

The hydration of C_2S is similar to the intensively studied hydration of C_3S; both yield C-S-H gel and portlandite ($Ca(OH)_2$) as hydration products.[10] β-C_2S is the most common polymorph of C_2S in cements. Using the original surface of the unreacted particle as a reference, C-S-H exhibits a distinct morphology in the outer and inner regions. The inner product (Ip) C-S-H from β-C_2S hydration is spherulite-like on the nanoscale,[11] while the outer product (Op) C-S-H is fibrillar[12] and contributes to the binding properties. Apart from the apparent morphological difference due to the available space for stacking,[11] there is no significant difference in composition between the Ip and Op.[12] The reactivity of β-C_2S is lower than that of C_3S, but the β-C_2S hydration is significant for the long-term performance of PC concrete.[13] The β-C_2S hydration has been investigated by nuclear magnetic resonance (NMR),[14−17] electron microscopy,[18−20] and other spectroscopies.[21−24] However, these techniques are not capable of locally probing the polymerization degree of the silicate chain of the Ip or Op; e.g., NMR, Raman spectroscopy, and infrared spectroscopy can provide chemical environmental Si of C-S-H, but are not capable of providing adequate spatial data.[25−27] Scanning electron microscopy provides high-resolution images, whereas the polymerization degree of C-S-H cannot be evaluated.[28] The potential artifacts generated by the harsh vacuum and high energy electron beam are also not completely understood.[29−31] Recently, α'_H-C_2S, another polymorph of C_2S, has increasingly gained research and industrial interests due to its higher hydration reactivity compared to β-C_2S.[32] However, the current understanding of the microchemistry (e.g., local coordination environment and silicate polymerization) during its hydration is limited.[33] Understanding the hydration of C_2S polymorphs and the structure of their hydration products C-S-H is essential for optimizing the properties of sustainable cement and concrete and for lowering the CO_2 emission and energy use in the construction industry.

Scanning transmission X-ray microscopy (STXM) is a powerful technique for characterizing the microchemistry of composite materials with a heterogeneous microstructure. It simultaneously provides morphological information and X-ray absorption near-edge structure (XANES) spectra of the elements of interest,[34,35] with a spatial resolution of up to 10 nm and a spectral resolution of 0.1 eV.[36] C-S-H gel is vulnerable to electron beam damage,[37] and the soft X-ray used in STXM (<2000 eV) is more likely to preserve the morphology of C-S-H.[38] The application of STXM in cement research started in recent years;[39−45] however, no STXM or XANES study has been reported on the hydration of C_2S.

In this work, the hydration products of C_2S polymorphs (β- and α'_H-) were studied by STXM at the Ca $L_{2,3}$- and Si K-edges. The coordination of Ca of anhydrous C_2S and C-S-H was also analyzed. Silicate polymerization of the Op and Ip and their C_2S interfaces at two different ages were locally probed. Ptychographic imaging was used to provide the interface morphology between the Ip and Op and between water and the Op with a spatial resolution of 10 nm.

MATERIALS AND METHODS

Preparation of β- and α'_H-C_2S. Chemical analytical grade $CaCO_3$, SiO_2, and K_2CO_3 were mixed according to the stoichiometric composition of $1.80CaO\text{-}0.10K_2O\text{-}SiO_2$ to prepare monoclinic β-C_2S. The mixed powder was calcined at 1500 °C for 3 h and then cooled in air.[46] Chemical analytical grade Ca_2SiO_4 and $Ca_3(PO_4)_2$ were stoichiometrically mixed as $1.946CaO\text{-}0.892SiO_2\text{-}0.054P_2O_5$ to prepare α'_H-C_2S. The mixed powder was sintered at 1450 °C for 6 h, followed by air cooling.[47] Note that, to ensure the fast formation of a single phase (high purity) of β- and α'_H-C_2S, the calcination temperatures of this laboratory synthesis were higher than typical calcination temperature of belite-rich cement (e.g., 1250 °C). The C_2S pellets were then ground into powders. The particle size distribution D-values, D10, D50, and D90 of anhydrous β-C_2S were 1.19 μm, 6.74 μm, and 18.48 μm, respectively. The D10, D50, and D90 of anhydrous α'_H-C_2S were 1.45 μm, 7.05 μm, and 19.08 μm, respectively.

Sample Preparation for STXM. Anhydrous C_2S powders were mixed with deionized water with a water-to-solid ratio (w/s) of 10 so that the particles were easily isolated by drop-casting to satisfy the transmission observation in the STXM. The suspensions were stored in polyethylene tubes filled with N_2 gas at 25 ± 1 °C. At early and late curing ages (10 days and 40 days for α'_H-C_2S; 17 days and 51 days for β-C_2S), the suspension of 0.5 μL was dropped onto a Si wafer frame (5 mm × 5 mm, 100 μm thick), where a 100 nm thick Si_3N_4 membrane window (1 mm × 1 mm, 100 nm thick) is in the center. The liquid was quickly and gently absorbed with a tip of KimWipes from the edge of the Si frame. The liquid removal process was monitored under an optical microscope to ensure that most of the solids remain on the membrane window. The anhydrous powders were dry-dusted on the Si_3N_4 membrane windows directly. These windows were then placed on the STXM sample stage inside a vacuum chamber.

Scanning Transmission X-ray Microscopy. The XANES spectra and images at Si K-edge (1830−1880 eV) and Ca $L_{2,3}$-edge (342−360 eV) were obtained at beamlines 5.3.2.1 and 5.3.2.2, respectively, at the Advanced Light Source of the Lawrence Berkeley National Laboratory (LBNL). Comprehensive descriptions of the STXM beamlines are given in refs 36 and 48.

The optical density (OD) at a specific energy of all pixels is affected by composition, density, and sample thickness.[40] Element mappings were obtained by differential measurements of the OD at pre- and on-edge at a spatial resolution up to 25 nm. Image stacks were collected by scanning the region of interest (ROI) at a series of beam energies, which yielded a XANES spectrum of each pixel on the ROI. RGB overlay maps, which visualize multiple phases with various compositions, were generated using singular value decomposition with reference spectra. All data processing was conducted using

DOI: 10.1021/acssuschemeng.8b05060
ACS Sustainable Chem. Eng. 2019, 7, 2316−2326

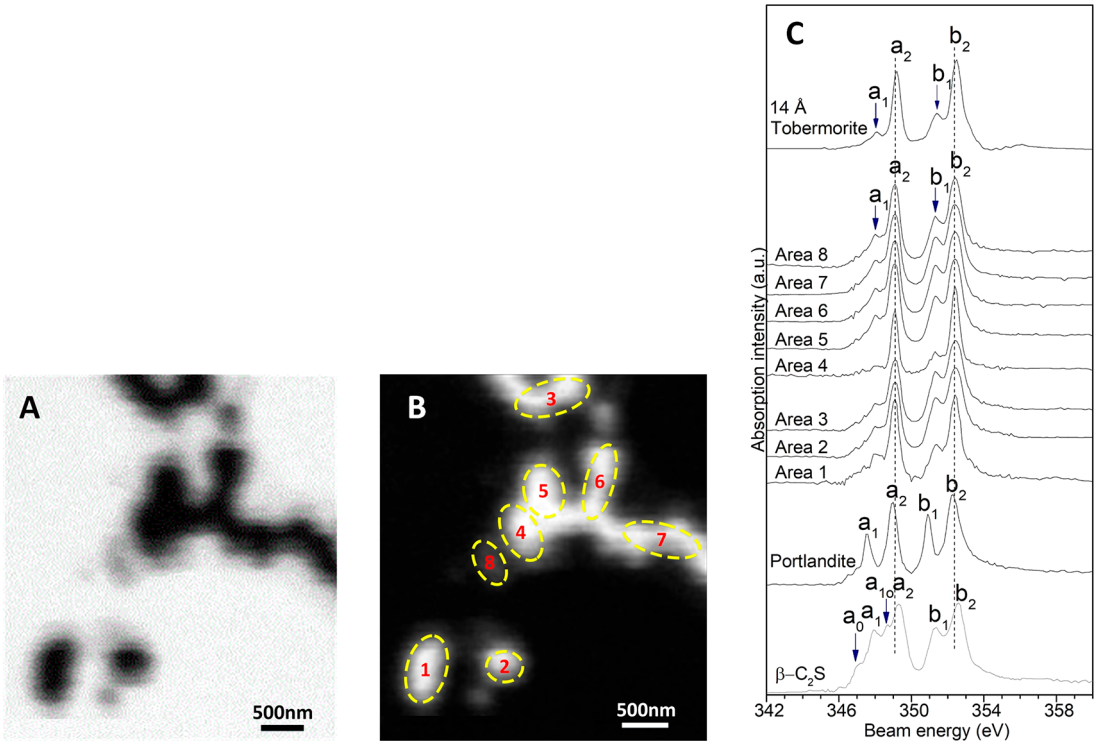

Figure 2. Hydrated β-C_2S at 17 days: (A) Transmission image of the ROI taken at 349 eV; (B) selected regions in the Ca element map for the XANES spectra; (C) Ca $L_{2,3}$-edge XANES spectra extracted from different regions specified in (B).

aXis2000 software.[48] At each age, at least two RGB maps were taken to obtain statistically reliable results, and at least 10 spectroscopic measurements were taken from different particles on each Si_3N_4 membrane.

Ptychographic images were collected at 800 eV at beamline 5.3.2.1. Full details of the imaging technique are given in ref 44. The spatial resolution of these transmission images is ~10 nm. The images were reconstructed by the Nanosurveyor package.[49] The width of C-S-H fibers of hydrated samples in the ptychographic images was quantified using ImageJ with F3D plugin developed at LBNL.[50]

RESULTS AND DISCUSSION

Ca Coordination of Anhydrous β-C_2S and Hydrated β-C_2S for 17 days. The Ca $L_{2,3}$-edge XANES spectra (Figure 2) consist of two major peaks, L_3 $2P_{3/2}$ (a_2) and L_2 $2P_{1/2}$ (b_2), which are due to the loss of degeneracy of 2p orbitals by spin–orbital interactions,[51] along with a number of minor leading peaks, a_0, a_1, and b_1, in order of increasing energy. The peak energy difference of a_2-a_1 and b_2-b_1 (ΔL_3 and ΔL_2, termed as splitting energy) and the intensity of the minor peaks are relevant to the coordination symmetry of Ca in the first shell and its ordering.[52−55]

The Ca $L_{2,3}$-edge XANES spectrum (Figure 2C) of anhydrous β-C_2S (monoclinic) exhibits a cubic-like symmetry with peak a_{1o} located between a_1 and a_2, and the peak energy differences of a_2-a_1 and b_2-b_1 are 1.54 and 1.2 eV, respectively. β-C_2S contains seven-fold and eight-fold coordinated Ca, denoted as Ca1 and Ca2 (Supporting Information, Figure S1). The equatorial plane of Ca1 is parallel to $(10\bar{1})$ with Ca–O bond lengths for Ca1 ranging from 2.273 to 2.892 Å with an average of 2.528 Å.[56] The five equatorial O atoms are not exactly coplanar. The Ca2 is coordinated by eight O atoms with a distorted symmetry for the cube, where the two trapezoids formed of the top four and bottom four O atoms are misaligned along each other's diagonal direction by 55°. The Ca–O bond lengths for Ca2 range from 2.400 to 2.676 Å with an average of 2.503 Å. The complex coordination of Ca1 and Ca2 in β-C_2S produces weak cubic-like crystal field splitting effects.

To avoid X-ray absorption saturation at low energy, only particles with a size of ~1 μm (Figure 2A, B) were measured at Ca $L_{2,3}$-edge. The 17-day hydrated β-C_2S grains at the Ca $L_{2,3}$-edge show mostly identical peak positions and an equivalent splitting energy in each grain, indicating that the Ca in each grain exhibits a similar environment. Peaks a_2 and b_2 in the selected areas are 0.1 eV lower than anhydrous β-C_2S, suggesting a lower bond strength of Ca–O. The splitting energies in the selected areas are 1.1 eV, suggesting a distorted octahedral-like symmetry for Ca.[52] The X-ray absorption features (i.e., splitting energy and peak positions) are similar to 14 Å tobermorite (calcium silicate hydrate mineral, $[Ca_4Si_6O_{16}(OH)_2{\cdot}2H_2O]{\cdot}(Ca{\cdot}5H_2O)$),[57,58] suggesting the C-S-H formed in this hydration system is structurally analogous to tobermorite. The relative intensity ratios of peak a_1-to-a_2 ($I(a_1)/I(a_2)$) and b_1-to-b_2 ($I(b_1)/I(b_2)$) of these selected areas are 0.021–0.041 and 0.050–0.077, respectively, which are lower than hydrothermally synthetic C-S-H at 25 °C (0.05–0.15 for $I(a_1)/I(a_2)$ and 0.07–0.15 for $I(b_1)/I(b_2)$).[38] The details in the calculation of relative intensity of these peaks are shown in Figure S2 (Supporting Information). Synthetic C-S-H has a longer range order than C-S-H formed in the β-C_2S hydration along the *c*-axis.[59] This suggests a shorter range order for Ca in this hydration system since the Ca/Si molar ratio of C-S-H in hydrated β-C_2S ranges from 1.2 to 2.1.[60] Moreover, no contribution by portlandite (a non-strength-giving phase in hydrated C_2S) was observed in the spectra, suggesting that C-S-H does not intermix with portlandite at the 25 nm scale in this ROI, and the interlayer six-fold coordinated Ca is also distorted. Thus, the Ca of C-S-H in hydrated β-C_2S

DOI: 10.1021/acssuschemeng.8b05060
ACS Sustainable Chem. Eng. 2019, 7, 2316–2326

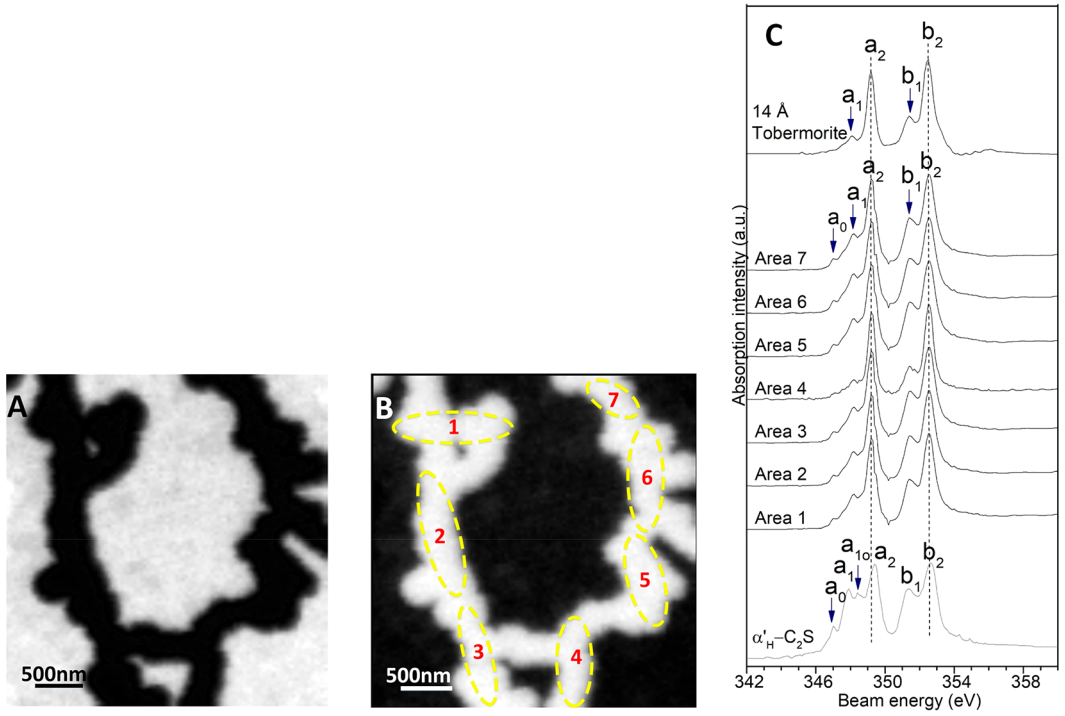

Figure 3. Hydrated α'_H-C_2S at 10 days: (A) Transmission image of the ROI taken at 349 eV; (B) selected regions in the Ca element map for the XANES spectra; (C) Ca $L_{2,3}$-edge XANES spectra extracted from different regions specified in (B).

is short-range-ordered and tobermorite-like. Portlandite crystallites were observed elsewhere in these dilute systems (Supporting Information, Figure S3).

Hydrated C_3S at 17 days also exhibited comparable peak positions, splitting energies, and intensity ratios in XANES at the Ca $L_{2,3}$-edge,[61] indicating that the Ca environment of hydrated C_3S is similar to that of hydrated β-C_2S. The extended X-ray absorption fine structure study showed that the Ca-O environment of hydrated β-C_2S is similar to that of 11 Å tobermorite, but the coordination number and Ca−O bond length of C-S-H could not be determined due to the presence of portlandite.[62] An ^{17}O NMR study demonstrated that Ca-OH sites are present in C-S-H of hydrated β-C_2S.[17] The C-S-H structure of hydrated β-C_2S proposed by Richardson[12] contains six- and seven-fold coordinated Ca in the interlayer and intralayer, respectively. The model proposed by Gartner[63] suggests that the interlayer Ca of C-S-H from hydration of C_3S and β-C_2S is six-fold coordinated. In the present work, the distorted six-fold Ca in the interlayer of hydrated β-C_2S fits both models.

Ca Coordination of Anhydrous α'_H-C_2S and α'_H-C_2S Hydrated for 10 Days. The Ca $L_{2,3}$-edge XANES spectra of α'_H-C_2S (orthorhombic) also exhibits a cubic-like symmetry with peak energy differences of a_2-a_1 of 1.57 eV and b_2-b_1 of 1.25 eV in Figure 3. This indicates a slightly stronger crystal field of Ca for α'_H-C_2S. α'_H-C_2S contains nine- and eight-fold coordinated Ca at two sites (denoted as Ca1 and Ca2; see Figure S1 in the Supporting Information) with Ca−O bond lengths for Ca1 ranging from 2.214 to 3.175 Å with an average of 2.708 Å, and those for Ca2 ranging from 2.292 to 2.927 Å with an average of 2.545 Å.[56] The superposition of symmetries and complex coordination leads to the cubic-like crystal field splitting of α'_H-C_2S. The energy difference in α'_H-C_2S is slightly larger compared to β-C_2S (monoclinic), suggesting that Ca-O complexes in α'_H-C_2S are more similar to cubic-like symmetry (less distorted) than in β-C_2S. For Ca1 in β-C_2S, its coordination number is seven, which is incapable of providing an ideal cubic symmetry.

Portlandite was not observed in this region for α'_H-C_2S hydrated for 10 days. Mostly identical peak positions and peak intensities were observed in each grain. Peaks a_2 and b_2 in the selected areas are ∼0.1 eV lower than for α'_H-C_2S, and the peak positions are 0.05 eV higher than for hydrated β-C_2S. The splitting energies in the compounds are ∼0.1 eV lower than for α'_H-C_2S but ∼0.05 eV higher than for hydrated β-C_2S. This suggests that the bond strength of Ca−O of hydrated α'_H-C_2S is slightly higher than that for hydrated β-C_2S; namely, more six-fold coordinated Ca is present in the α'_H-C_2S hydration system. The intensity ratios of hydrated α'_H-C_2S are 0.018−0.038 and 0.037−0.067, which are also lower than for anhydrous but comparable to or slightly lower than hydrated β-C_2S. These absorption features indicate that the coordination symmetry of Ca in hydrated α'_H-C_2S is also tobermorite-like, but the ordering of Ca is slightly lower than for hydrated β-C_2S.

Si Environment of Anhydrous β-C_2S and β-C_2S Hydrated for 17 Days. The major peak of a_1 at the Si K-edge of β-C_2S (Figure 4C) is assigned to the electronic excitation from 1s to the antibonding 3p-like state orbital (t_2) of tetrahedral Si.[64,65] Pre-edge peak a_0 is attributed to the dipole-forbidden transition of 1s electrons to the antibonding 3s-like states.[66] This forbidden peak appears due to the mixing of s- and p-states when the SiO_4 tetrahedra coordination is highly distorted. Thus, the intense a_0 peak of β-C_2S suggests a strong distortion of the silicate tetrahedron. The minor peak of a_2 is assigned to the multiple-scattering effect from more distant atom shells through a photoelectron interaction; its energy is governed by the interatomic distance and structural complexity.[67]

DOI: 10.1021/acssuschemeng.8b05060
ACS Sustainable Chem. Eng. 2019, 7, 2316−2326

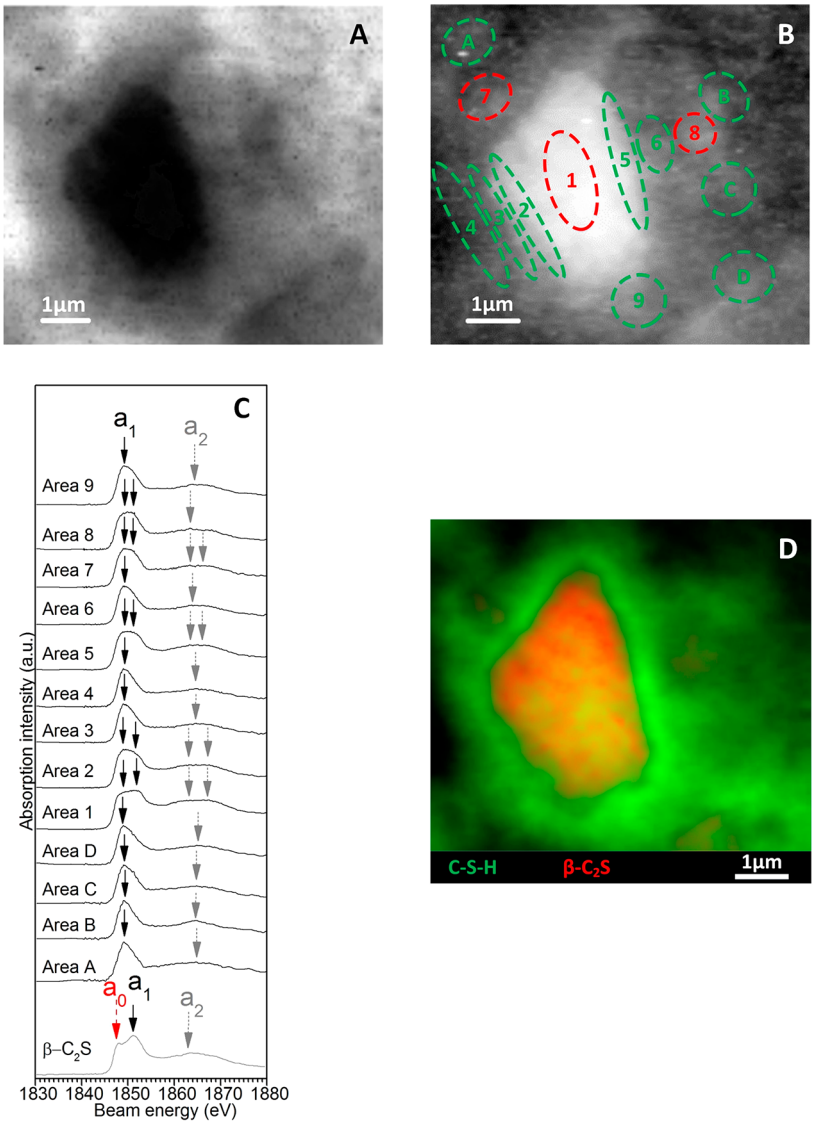

Figure 4. Hydrated β-C_2S at 17 days: (A) Transmission image of the ROI taken at 1849 eV; (B) selected regions in the Si element map from the XANES spectra; (C) Si *K*-edge XANES spectra extracted from different regions specified in (B); (D) RGB overlay map using XANES spectra obtained from the C-S-H (Area 4, green) marked in (B) and reference spectrum of anhydrous β-C_2S (red). More RGB over maps can be found in Figure S4 (Supporting Information).

The interface between the β-C_2S core and the hydrous layer C-S-H is well distinguished (Figure 4), indicating changes in the phase density. The OD of the hydration product layer slightly decreases with increasing distance from the interface, which is associated with several small brighter regions. Compared to the C_3S hydration system,[61] the C-S-H of hydrated β-C_2S is more dispersed, and fibrils are not present at this age and at this resolution (Figure 4A).

Peak a_1 is not shown at ~1851.1 eV in areas 3, 4, 6, but a single a_1 peak is at 1848.8 eV in these areas (Figure 4C), suggesting that C-S-H is the only silicate phase in these areas. The absorption features of C-S-H in hydrated β-C_2S resemble those of C-S-H in C_3S hydration systems.[43,61,64] The Si *K*-edge (a_1 peak) at 1848.8 eV of C-S-H is 2.2 eV lower than that of β-C_2S due to the longer Si−O bond of the C-S-H relative to β-C_2S.[56,69] Li[64] concluded that, although there is considerable overlapping for silicate minerals with different polymerization types, the Si *K*-edge generally shifts to higher energy with increased silicate polymerizations. Thus, in this case, the Si−O bond length, rather than the polymerization degree, dominates the Si *K*-edge shift.

The energy difference between a_1 and a_2, $\Delta a_2 - a_1$, can be used to evaluate the degree of silicate polymerization.[38,43,61,68] The values of $\Delta a_2 - a_1$ for areas 3 and 4 are equivalent, suggesting that the degree of polymerization of the C-S-H here is comparable. The energy positions of multiple scattering peaks (e.g., a_2) are affected by the Si interatomic distances, while the intensity and number of resonances are heavily dependent on the bond angle, site symmetry, and number of nearest neighboring oxygen atoms (Si in most cement phases are four-fold coordinated, expect thaumasite, where Si is six-fold coordinated).[70] Two a_2 peaks are distinguished in the spectra in areas 2 and 5. In these areas, a peak at 1848.8 eV and a broad shoulder/hump at ~1851.1 eV were observed. The peak is assigned to the a_1 peak of C-S-H, and the shoulder/hump is the contribution of the a_1 peak (at 1851.0 eV) of anhydrous β-C_2S. These absorption features suggest that areas 2 and 5 are mixtures of C-S-H and anhydrous β-C_2S, and the

DOI: 10.1021/acssuschemeng.8b05060
ACS Sustainable Chem. Eng. 2019, 7, 2316−2326

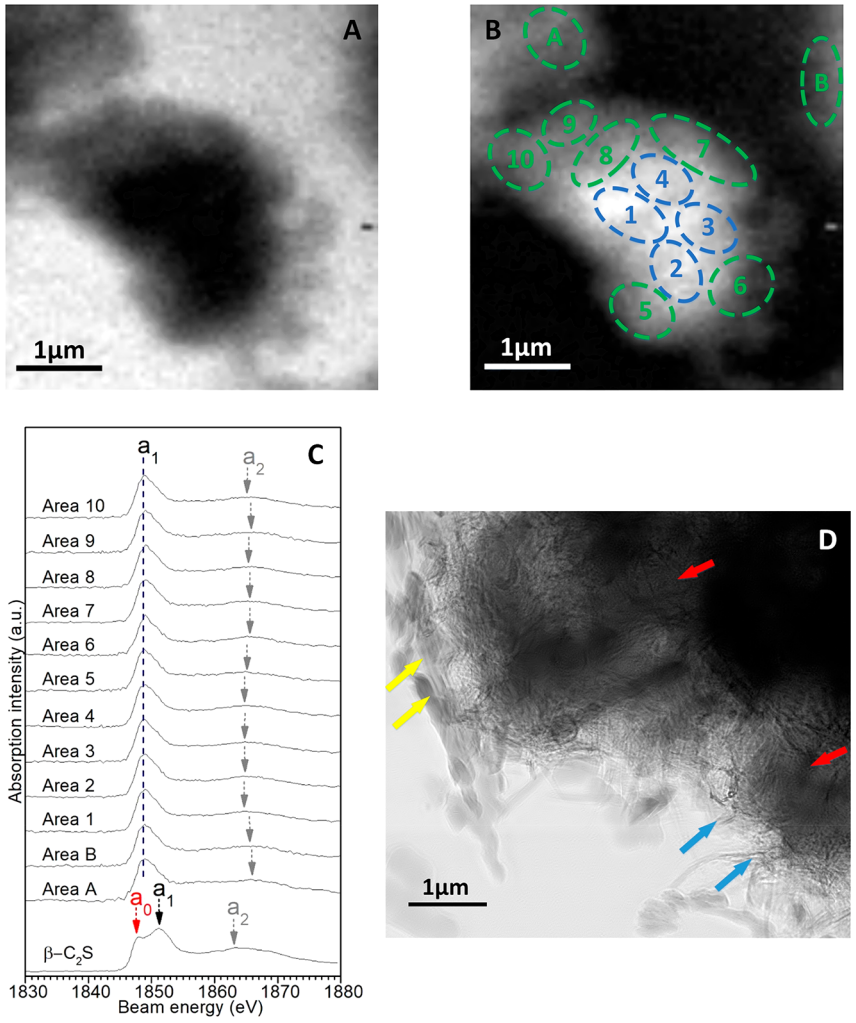

Figure 5. Hydrated β-C_2S at 51 days: (A) Transmission image of the ROI at 1849 eV; (B) selected regions in the Si element map for the XANES spectra; (C) Si *K*-edge XANES spectra extracted from different regions specified in (C); (D) ptychographic image of another area at the same age. Op is indicated by blue arrows, Ip is indicated by red arrows, and portlandite is indicated by yellow arrows.

hydration here is incomplete. Similarly, areas 7 and 8 are mixes of C-S-H and anhydrous β-C_2S, implying that small β-C_2S particles exist in these areas. This fact is consistent with the original granulometry result of β-C_2S; ~10% of β-C_2S was below 1 μm. Note that a weak contribution of C-S-H to the spectrum at ~1848.8 eV is observed in area 1 since C-S-H surrounds the entire grain. $\Delta a_2 - a_1$ of area 6 is 0.9 eV lower than those of areas 3 and 4 (~15.7 eV), suggesting a lower degree of polymerization of C-S-H in the area. The difference in local polymerization degree can be explained by the different dissolution rates on the crystal faces and by different numbers of surface defects of β-C_2S;[71] multiple crystal faces with low hydraulic reactivity occur in area 6. Note that, hydraulic reactivity of all faces of pure β-Ca_2SiO_4 is similar; the dopant changes the local reactivity of β-C_2S crystals.[72] Similarly, the value of $\Delta a_2 - a_1$ for C-S-H in area 9 is 0.7 eV lower than that for C-S-H in the unconstrained space. The RGB overlay map (Figure 4D) shows that the C-S-H surrounds the unreacted core, which is consistent with the analysis above. The values of $\Delta a_2 - a_1$ for C-S-H among different grains (Areas A–D) are 15.6–16.1 eV, indicating a distinction in silicate polymerization due to the interference of other grains and the hydration rate. In addition, the contribution of cross-linking sites to the spectra is not observed in the typical range at 1853–1854 eV[73] since the basal layers of C-S-H are separated by $[Ca(H_2O)_6]^{2+}$ or $[Ca(OH)(H_2O)_5]^{+}$.[63] ^{29}Si NMR studies showed that the mean silicate chain lengths of C-S-H of 7–12 months hydrated β-C_2S are still lower than 3.5.[12,74] This suggests that the proportion of long silicate chains (octamer or longer) in this C-S-H is relatively low. Therefore, the C-S-H at 17 days is mainly a mixture of dimer and pentamer C-S-Hs.

It is well-known that the degree of silicate polymerization of synthetic C-S-H increases as Ca/Si decreases.[26,27] Although the degree of polymerization of hydrated β-C_2S progressively increases over time,[17,75] there is no significant variation in the mean Ca/Si of Op (excluding intermixed portlandite) with age.[37] Thus, it is difficult to estimate the local degree of polymerization based on Ca/Si ratio. STXM is a more reliable technique to locally probe the variation in silicate polymerization of the C-S-H without considering intermixed microcrystalline portlandite in the hydrous regions[12] and unreacted β-C_2S.

Si Environment of Hydrated β-C_2S for 51 Days. Two distinct optical densities were observed at 51 days (Figure 5A). Double a_1 peaks are not observed in Figure 5B, and only a single a_1 peak at 1848.9–1849.1 eV occurs. Peak a_0 at 1847.9 eV was not observed, suggesting a fully hydrated grain (see Supporting Information, Figure S5). The peak difference of

DOI: 10.1021/acssuschemeng.8b05060
ACS Sustainable Chem. Eng. 2019, 7, 2316–2326

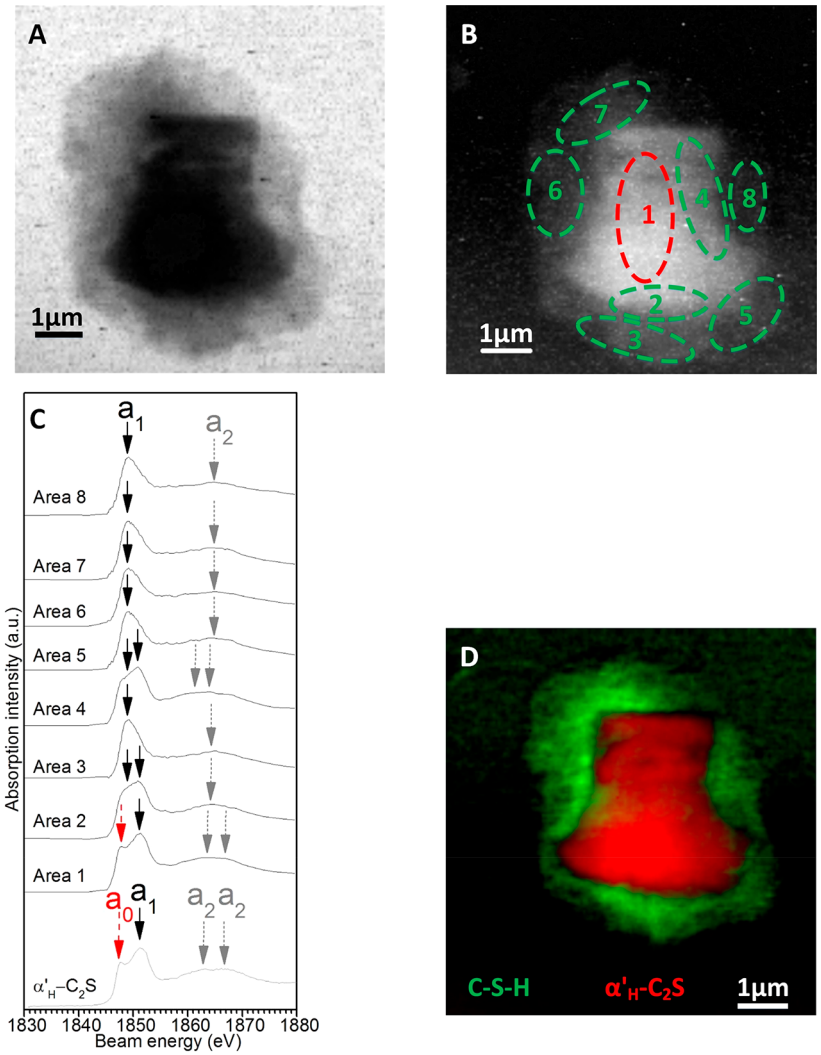

Figure 6. Hydrated α'_H-C_2S at 10 days: (A) Transmission image of the ROI taken at 1849 eV; (B) selected regions in the Si element map for the XANES spectra; (C) Si *K*-edge XANES spectra extracted from different regions specified in (B); (D) RGB overlay map using XANES spectra obtained from the C-S-H (Area 7, green) marked in (B) and reference spectrum of anhydrous α'_H-C_2S (red).

Δa_2-a_1 for areas 5, 6, 7, 8, 9, and B is 16.7−17.0 eV, and 15.8−16.2 eV for areas 1, 2, 3, and 4; two distinct ranges of Δa_2-a_1 are observed in Figure 5C. Thus, the two distinct ODs indicate the existence of Ip (dark region) and Op (light region) in Figure 5A. Areas 5, 6, 7, 8, and 9 are Ip dominant, while the areas 1, 2, 3, and 4 are Op dominant. The Si *K*-edge (a_1) and Δa_2-a_1 of Ip are both lower compared to those of Op, indicating a lower silicate polymerization and a slightly longer Si−O bond for Ip. The Δa_2-a_1 and Si *K*-edge for Op at 51 days are slightly higher than at 17 days, revealing that the Op polymerizes over time. The lower Δa_2-a_1 for areas 10 and A may be explained by impingement from adjacent grains. Similarly, contribution of cross-linking sites to the spectra was also not observed due to the abundant interlayer Ca between basal layers of C-S-H.[63] Thus, both Op and Ip are likely mixtures of dimer and pentamer C-S-Hs with very small amounts of octamer and longer chains. The values of Δa_2-a_1 for Op and Ip are larger compared to those of synthetic C-S-H with a bulk Ca/Si molar ratio of 1.4,[38] suggesting that the electron shielding on Si from cations in hydration product C-S-Hs is weaker. This can be explained by the highly distorted Ca of $[Ca(OH)(H_2O)_5]^+$ in the interlayer of C-S-Hs, and the partial replacement of divalent Ca by monovalent K from the dopant.[76] Future study will focus on the coordination environment of K in this system and the electron density around these atoms.

The ptychographic image (Figure 5D) shows the fibrillar Op of another hydrated β-C_2S particle at 51 days; the width of fibers has a distribution of 11−25 nm, which is smaller than the Op of C_3S.[77] The Ip of β-C_2S exhibits a dense aggregated structure, and the Ip of C_3S with the same w/s exhibits a less dense structure with aggregates of globules.[77] The morphological difference between the two Ip's can be explained by the lower reactivity of β-C_2S. Geng[68] reported that the Ip and Op of hydrated C_3S exhibit an identical Si *K*-edge with a higher energy for the a_2 peaks of Op, showing that Ip has a lower degree of silicate polymerization. Portlandite microcrystallites intermixed with Op is observed, which is consistent with TEM study of Richardson.[11]

Si Environment of Anhydrous and Hydrated α'_H-C_2S for 10 Days. Similar to β-C_2S, pre-edge peak a_0 was also observed in α'_H-C_2S (Figure 6C), suggesting a slight distortion of the silicate tetrahedron of α'_H-C_2S. The Si *K*-edge of α'_H-C_2S is 0.2 eV higher than for β-C_2S, suggesting a slightly

DOI: 10.1021/acssuschemeng.8b05060
ACS Sustainable Chem. Eng. 2019, 7, 2316−2326

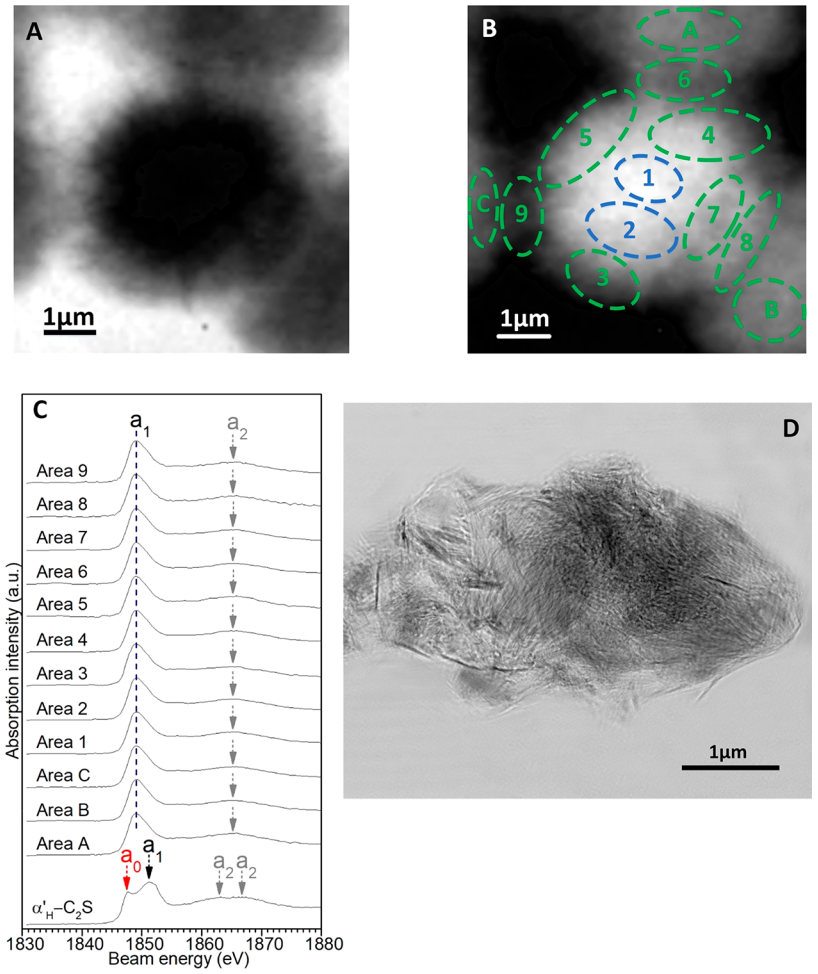

Figure 7. Hydrated α'_H-C_2S at 40 days: (A) Transmission image of the ROI taken at 1849 eV; (B) selected regions in the Si element map for the XANES spectra; (C) Si *K*-edge XANES spectra extracted from different regions specified in (B); (D) ptychographic image.

shorter Si−O bond for α'_H-C_2S compared with β-C_2S, which is consistent with XRD refinement.[56]

Similar to β-C_2S hydration, the interface between non-fibrillar Op and α'_H-C_2S was observed at 10 days (Figure 6). The Si *K*-edge and $\Delta a_2 - a_1$ of hydrated α'_H-C_2S at 10 days are equivalent to or 0.2−0.3 eV larger than that for hydrated β-C_2S at 17 days. Thus, the chemical environment of Si in hydrated α'_H-C_2S is similar to that in β-C_2S hydration at 17 days with a comparable degree of polymerization at an earlier age. The polymerization degree of the Op is more homogeneous since the $\Delta a_2 - a_1$ values of all C-S-Hs here are ∼15.9 eV. Again, Op cross-linking sites are not present, suggesting that the Op is still mainly a mixture of dimer and pentamer units.[18] Thus, α'_H-C_2S exhibits a higher reactivity relative to β-C_2S. This work is consistent with experimental and simulation studies on the reactivity[32,47,78] but provides new details on the rate of polymerization of α'_H-C_2S hydration.

Si Environment of Hydrated α'_H-C_2S for 40 Days. The C-S-H of α'_H-C_2S at 40 days is fibrillar in Figure 7. There was no Ip/Op interface in the fully hydrated grain (see Supporting Information, Figure S6) observed. The values of $\Delta a_2 - a_1$ for all the areas range from 16.7 to 17.0 eV, suggesting a relatively homogeneous polymerization. This is a primary difference compared to β-C_2S. The Si *K*-edge (a_1) of all areas is comparable, suggesting similar Si coordination in these areas. The comparable degree of polymerization of the interfaces between different grains suggests that the polymerization is not obviously interfered by adjacent grains. Additionally, the C-S-Hs are mainly mixtures of dimer and pentamer units, and a cross-linking effect was not observed on the spectra. Compared to the Op of β-C_2S at 51 days, hydrated α'_H-C_2S at 40 days exhibited a comparable polymerization degree at an earlier age. This confirms the higher reactivity of α'_H-C_2S compared with β-C_2S.

The ptychographic image (Figure 7D) shows the fibrillar C-S-H with a width of 15−30 nm, which is larger than hydrated β-C_2S but smaller than hydrated C_3S (41−59 nm),[77] and the inner C-S-H exhibits a looser aggregated structure with ∼17 nm voids compared to the Ip of hydrated β-C_2S. The Ip's of hydrated β-C_2S, C_3S, and PC with a practical w/s (i.e., <0.6) appear to be small and globular.[79] The larger void of the Ip relative to the Ip of hydrated C_3S[79] could be induced by the w/s of 10 used in this study, which provides sufficient space for nanocrystallite growth during the fast hydration. The microstructure of hydrated α'_H-C_2S is similar to that of hydrated C_3S with the same w/s[77] instead of the hydrated β-C_2S mentioned above. Thus, the morphological difference among the silicates in these diluted systems may be relevant to their hydration reactivity. More ptychographic images can be found in Figure S7 (Supporting Information).

DOI: 10.1021/acssuschemeng.8b05060
ACS Sustainable Chem. Eng. 2019, 7, 2316−2326

CONCLUSIONS

The coordination environments of Ca and Si in anhydrous β-C_2S, α'_H-C_2S, and their hydration products were studied using STXM; the morphology of C-S-Hs was imaged by ptychography. The key conclusions are

(1) Ca in both anhydrous phases are in a distorted cubic symmetric coordination. The Ca coordination of C-S-H in both hydration systems is highly distorted and is similar to 14 Å tobermorite but have a shorter-range order. More six-fold coordinated Ca occur in hydrated α'_H-C_2S than in hydrated β-C_2S.

(2) The Si of both anhydrous phases have asymmetric tetrahedral coordination. The silicate chain of the Op in both hydration systems polymerizes over time. The hydration products in the α'_H-C_2S system polymerize faster than in β-C_2S. The hydraulic reactivity of α'_H-C_2S is higher.

(3) Ip has a lower degree of silicate polymerization than Op in fully hydrated β-C_2S, which is accompanied by a slightly longer Si−O bond due to the space constraint for contacting water. Compared with hydrated β-C_2S, the silicate polymerization in hydrated α'_H-C_2S is more homogeneous.

(4) The C-S-H of hydrated β-C_2S exhibits fine fibrils that intermix with portlandite, and Ip appears to be a dense aggregated structure. The morphology of fully hydrated α'_H-C_2S is more homogeneous, and its inner region is slightly more porous with nanosize voids. Ip and Op are not distinguished in fully hydrated α'_H-C_2S

Therefore, this study provides insights into advanced applications of the hydration behaviors of C_2S to C_2S rich cements and the controllability of the performance of these materials in service. The lower calcination temperature and CO_2 emission of α'_H-C_2S during manufacturing can reduce the environmental impact of cement manufacturing. Due to its high reactivity, α'_H-C_2S can be a practical alternative to C_3S and β-C_2S in Portland cement or BCSA cement. Therefore, this work is an important step toward the development of the hydration mechanism of C_2S-rich cement, which will provide new insight into the performance of these sustainable cements (lower CO_2 emission and energy use) in service.

ASSOCIATED CONTENT

Supporting Information

The Supporting Information is available free of charge on the ACS Publications website at DOI: 10.1021/acssuschemeng.8b05060.

Coordination environment of Ca in two C_2S polymorphs; an example of fitting of a XANES spectrum at Ca $L_{2,3}$-edge; transmission images at 349 eV of samples at 10 and 17 days; RGB overlay maps of samples at 10, 17, 40, and 51 days; ptychographic images of samples at 40 and 51 days (PDF)

AUTHOR INFORMATION

Corresponding Author

*E-mail: guoqing_geng@berkeley.edu.

ORCID

Guoqing Geng: 0000-0003-2862-4774

Paulo J. M. Monteiro: 0000-0002-6866-1783

Author Contributions

J.L., G.G., and P.J.M.M. conceived and designed the experiments. J.L. conducted the experiments. Y.-S.Y. and D.A.S. supported the imaging experiments. J.L., G.G., and W.Z. analyzed the results. J.L. and G.G. wrote the manuscript. All authors reviewed the manuscript.

Notes

The authors declare no competing financial interest.

ACKNOWLEDGMENTS

This research was founded by the Republic of Singapore's National Research Foundation through a grant to the Berkeley Education Alliance for Research in Singapore (BEARS) for the Singapore-Berkeley Building Efficiency and Sustainability in the Tropics (SinBerBEST) Program. The Advanced Light Source is supported by the Director, Office of Science, and Office of Basic Energy Sciences of the U.S. Department of Energy under Contract No. DE-AC02-05CH11231. G.G. also wants to acknowledge European Union's Horizon 2020 research and innovation programme under the Marie Skłodowska-Curie grant agreement No. 701647. We thank Matthew Marcus for insightful discussions on fitting and interpretation of Ca $L_{2,3}$-edge XANES spectra. We thank Ellis Gartner for the personal communication and help on the study of dicalcium silicates.

REFERENCES

(1) Myers, R. J.; Geng, G.; Li, J.; Rodriguez, E. D.; Ha, J. Y.; Kidkhunthod, P.; Sposito, G.; Lammers, L. N.; Kirchheim, A. P.; Monteiro, P. J. M. Role of adsorption phenomena in cubic tricalcium aluminate dissolution. *Langmuir* **2017**, *33* (1), 45−55.

(2) Mehta, P. K. Reducing the environmental impact of concrete. *Concr. Int.* **2001**, *23* (10), 61−66.

(3) Lee, B. Y.; Kurtis, K. E. Proposed acceleratory effect of TiO_2 nanoparticles on belite hydration: Preliminary results. *J. Am. Ceram. Soc.* **2012**, *95* (1), 365−368.

(4) Chen, I. A.; Hargis, C. W.; Juenger, M. C. G. Understanding expansion in calcium sulfoaluminate-belite cements. *Cem. Concr. Res.* **2012**, *42* (1), 51−60.

(5) Quillin, K. Performance of belite-sulfoaluminate cements. *Cem. Concr. Res.* **2001**, *31* (9), 1341−1349.

(6) Zhou, Y.; Hou, D.; Jiang, J.; She, W.; Li, J. Molecular dynamics study on the solvated aniline (AN) and ethylene glycol (EG) monomers confined in calcium silicate nanometer channel: A case study of tobermorite. *Phys. Chem. Chem. Phys.* **2017**, *19*, 15145.

(7) Hou, D. S.; Zhang, J. R.; Li, Z. J.; Zhu, Y. Uniaxial tension study of calcium silicate hydrate (C-S-H): Structure, dynamics and mechanical properties. *Mater. Struct.* **2015**, *48* (11), 3811−3824.

(8) Merlino, S.; Bonaccorsi, E.; Kampf, A. R. Tobermorite 14 angstrom: Crystal structure and od character. *Appl. Mineral.* **2000**, *1-2*, 859−861.

(9) Geng, G.; Myers, R. J.; Li, J.; Maboudian, R.; Carraro, C.; Shapiro, D. A.; Monteiro, P. J. Aluminum-induced dreierketten chain cross-links increase the mechanical properties of nanocrystalline calcium aluminosilicate hydrate. *Sci. Rep.* **2017**, *7*, 44032.

(10) Guo, P.; Wang, B.; Bauchy, M.; Sant, G. Misfit stresses caused by atomic size mismatch: The origin of doping-induced destabilization of dicalcium silicate. *Cryst. Growth Des.* **2016**, *16* (6), 3124−3132.

(11) Richardson, I. G. The nature of C-S-H in hardened cements. *Cem. Concr. Res.* **1999**, *29* (8), 1131−1147.

(12) Richardson, I. G. Tobermorite/jennite- and tobermorite/calcium hydroxide-based models for the structure of C-S-H: Applicability to hardened pastes of tricalcium silicate, beta-dicalcium silicate, portland cement, and blends of portland cement with blast-

fumace slag, metakaolin, or silica fume. *Cem. Concr. Res.* **2004**, *34* (9), 1733−1777.
(13) Taylor, H. F. W. *Cement Chemistry*; Thomas Telford: London, 1997.
(14) Chen, J. H.; Wang, Y. Y.; Wan, C. C.; Liou, D. C. MAS NMR-studies of the hydration process of beta-C_2S in the presence of chromium. *Cem. Concr. Res.* **1994**, *24* (2), 319−324.
(15) Tong, Y. Y.; Du, H.; Fei, L. Hydration process of beta-dicalcium silicate followed by MAS and CP/MAS nuclear-magnetic-resonance. *Cem. Concr. Res.* **1991**, *21* (2−3), 355−358.
(16) Tong, Y. Y.; Du, H.; Fei, L. CP-MAS NMR-studies of the initial hydration processes of activated and ordinary beta-dicalcium silicates. *Cem. Concr. Res.* **1990**, *20* (6), 986−991.
(17) Cong, X.; Kirkpatrick, R. J. 17O and 29Si MAS NMR study of β−C_2S hydration and the structure of calcium-silicate hydrates. *Cem. Concr. Res.* **1993**, *23* (5), 1065−1077.
(18) Richardson, I. G. The nature of the hydration products in hardened cement pastes. *Cem. Concr. Compos.* **2000**, *22* (2), 97−113.
(19) Doval, M.; Palou, M.; Mojumdar, S. C. Hydration behavior of C_2S and C_2AS nanomaterials, synthetized by sol-gel method. *J. Therm. Anal. Calorim.* **2006**, *86* (3), 595−599.
(20) Lawrence, F. V.; Reid, D. A.; De Carvalho, Aa Transmission electron-microscopy of hydrated dicalcium silicate thin-films. *J. Am. Ceram. Soc.* **1974**, *57* (3), 144−148.
(21) Ibanez, J.; Artus, L.; Cusco, R.; Lopez, A.; Menendez, E.; Andrade, M. C. Hydration and carbonation of monoclinic C_2S and C_3S studied by raman spectroscopy. *J. Raman Spectrosc.* **2007**, *38* (1), 61−67.
(22) Delgado, A. H.; Paroli, R. M.; Beaudoin, J. J. Comparison of IR techniques for the characterization of construction cement minerals and hydrated products. *Appl. Spectrosc.* **1996**, *50* (8), 970−976.
(23) Rheinheimer, V.; Casanova, I. An X-ray photoelectron spectroscopy study of the hydration of C_2S thin films. *Cem. Concr. Res.* **2014**, *60*, 83−90.
(24) Black, L.; Stumm, A.; Garbev, K.; Stemmermann, P.; Hallam, K. R.; Allen, G. C. X-ray photoelectron spectroscopy of the cement clinker phases tricalcium silicate and beta-dicalcium silicate. *Cem. Concr. Res.* **2003**, *33* (10), 1561−1565.
(25) Ortaboy, S.; Li, J.; Geng, G.; Myers, R. J.; Monteiro, P. J.; Maboudian, R.; Carraro, C. Effects of CO_2 and temperature on the structure and chemistry of C−(A−) S−H investigated by raman spectroscopy. *RSC Adv.* **2017**, *7* (77), 48925−48933.
(26) Yu, P.; Kirkpatrick, R. J.; Poe, B.; McMillan, P. F.; Cong, X. D. Structure of calcium silicate hydrate (C-S-H): Near-, mid-, and far-Infrared spectroscopy. *J. Am. Ceram. Soc.* **1999**, *82* (3), 742−748.
(27) Cong, X. D.; Kirkpatrick, R. J. Si-29 MAS NMR study of the structure of calcium silicate hydrate. *Adv. Cem. Based Mater.* **1996**, *3* (3−4), 144−156.
(28) Zhou, Y.; She, W.; Hou, D.; Yin, B.; Chang, H.; Jiang, J.; Li, J. Modification of incorporation and in-situ polymerization of aniline on the nano-structure and meso-structure of calcium silicate hydrates. *Construction and Building Materials* **2018**, *182*, 459−468.
(29) Gallucci, E.; Mathur, P.; Scrivener, K. Microstructural development of early age hydration shells around cement grains. *Cem. Concr. Res.* **2010**, *40* (1), 4−13.
(30) Collier, N. C.; Sharp, J. H.; Milestone, N. B.; Hill, J.; Godfrey, I. H. The influence of water removal techniques on the composition and microstructure of hardened cement pastes. *Cem. Concr. Res.* **2008**, *38* (6), 737−744.
(31) Galle, C. Effect of drying on cement-based materials pore structure as identified by mercury intrusion porosimetry - a comparative study between oven-, vacuum-, and freeze-drying. *Cem. Concr. Res.* **2001**, *31* (10), 1467−1477.
(32) Cuesta, A.; Losilla, E. R.; Aranda, M. A.; Sanz, J.; De la Torre, A. Reactive belite stabilization mechanisms by boron-bearing dopants. *Cem. Concr. Res.* **2012**, *42* (4), 598−606.
(33) Ghose, A.; Chopra, S.; Young, J. F. Microstructural characterization of doped dicalcium silicate polymorphs. *J. Mater. Sci.* **1983**, *18* (10), 2905−2914.
(34) Yano, J.; Yachandra, V. K. X-ray absorption spectroscopy. *Photosynth. Res.* **2009**, *102* (2−3), 241−254.
(35) Chae, S. R.; et al. Advanced nanoscale characterization of cement based materials using x-ray synchrotron radiation: A review. *Int. J. Concr. Struct. Mater.* **2013**, *7* (2), 95−110.
(36) Kilcoyne, D. A new scanning transmission X-ray microscope at the ALS for operation up to 2500 eV. *AIP Conf. Proc.* **2009**, *1234*, 465.
(37) Richardson, I. G.; Groves, G. W. Microstructure and microanalysis of hardened ordinary portland-cement pastes. *J. Mater. Sci.* **1993**, *28* (1), 265−277.
(38) Li, J.; Geng, G.; Myers, R. J.; Yu, Y.-S.; Shapiro, D.; Carraro, C.; Maboudian, R.; Monteiro, P. J. M. The chemistry and structure of calcium (alumino) silicate hydrate: A study by xanes, ptychographic imaging, and wide- and small- angle scattering. *Cem. Concr. Res.* **2019**, *115*, 367−378.
(39) Wieland, E.; Dahn, R.; Vespa, M.; Lothenbach, B. Micro-spectroscopic investigation of Al and S speciation in hardened cement paste. *Cem. Concr. Res.* **2010**, *40* (6), 885−891.
(40) Ha, J.; Chae, S.; Chou, K. W.; Tyliszczak, T.; Monteiro, P. J. M. Effect of polymers on the nanostructure and on the carbonation of calcium silicate hydrates: A scanning transmission X-ray microscopy study. *J. Mater. Sci.* **2012**, *47* (2), 976−989.
(41) Ha, J.; Chae, S.; Chou, K. W.; Tyliszczak, T.; Monteiro, P. J. M. Scanning transmission X-ray microscopic study of carbonated calcium silicate hydrate. *Transp. Res. Rec.* **2010**, *2142* (2142), 83−88.
(42) Hernandez-Cruz, D.; Hargis, C. W.; Bae, S.; Itty, P. A.; Meral, C.; Dominowski, J.; Radler, M. J.; Kilcoyne, D. A.; Monteiro, P. J. M. Multiscale characterization of chemical-mechanical interactions between polymer fibers and cementitious matrix. *Cem. Concr. Compos.* **2014**, *48*, 9−18.
(43) Li, Q.; Ge, Y.; Geng, G.; Bae, S.; Monteiro, P. J. M. $CaCl_2$-accelerated hydration of tricalcium silicate: A stxm study combined with 29Si MAS NMR. *J. Nanomater.* **2015**, *2015*, 1−10.
(44) Geng, G.; Myers, R. J.; Yu, Y. S.; Shapiro, D. A.; Winarski, R.; Levitz, P. E.; Kilcoyne, D. A. L.; Monteiro, P. J. M. Synchrotron X-ray nanotomographic and spectromicroscopic study of the tricalcium aluminate hydration in the presence of gypsum. *Cem. Concr. Res.* **2018**, *111*, 130−137.
(45) Geng, G.; Myers, R. J.; Kilcoyne, A. L.; Ha, J.; Monteiro, P. J. Ca $L_{2,3}$-edge near edge X-ray absorption fine structure of tricalcium aluminate, gypsum, and calcium (sulfo) aluminate hydrates. *Am. Mineral.* **2017**, *102* (4), 900−908.
(46) Lai, G. C.; Nojiri, T.; Nakano, K. Studies of the stability of beta-Ca_2SiO_4 doped by minor ions. *Cem. Concr. Res.* **1992**, *22* (5), 743−754.
(47) Müller, R.; Neubauer, J.; Götz-Neunhoeffer, F. Effects of phosphate rich raw materials on the crystallographic and hydraulic properties of dicalcium silicate. In *Proceedings of the 11th International Congress on the Chemistry of Cement*, Durban, South Africa, May 11−16, 2003; Tech Books International, 2003; pp 1045−1053.
(48) Kilcoyne, A. L. D.; Tyliszczak, T.; Steele, W. F.; Fakra, S.; Hitchcock, P.; Franck, K.; Anderson, E.; Harteneck, B.; Rightor, E. G.; Mitchell, G. E.; Hitchcock, A. P.; Yang, L.; Warwick, T.; Ade, H. Interferometer-controlled scanning transmission x-ray microscopes at the advanced light source. *J. Synchrotron Radiat.* **2003**, *10*, 125−136.
(49) Shapiro, D. A.; Yu, Y.-S.; Tyliszczak, T.; Cabana, J.; Celestre, R.; Chao, W.; Kaznatcheev, K.; Kilcoyne, A. D.; Maia, F.; Marchesini, S.; et al. Chemical composition mapping with nanometre resolution by soft X-ray microscopy. *Nat. Photonics* **2014**, *8* (10), 765−769.
(50) Ushizima, D. M.; Bale, H. A.; Bethel, E. W.; Ercius, P.; Helms, B. A.; Krishnan, H.; Grinberg, L. T.; Haranczyk, M.; Macdowell, A. A.; Odziomek, K.; Parkinson, D. Y.; Perciano, T.; Ritchie, R. O.; Yang, C. Ideal: Images across domains, experiments, algorithms and learning. *JOM* **2016**, *68* (11), 2963−2972.
(51) De Groot, F. M. F.; Fuggle, J. C.; Thole, B. T.; Sawatzky, G. A. 2p X-ray absorption of 3d transition-metal compounds - an atomic multiplet description including the crystal-field. *Phys. Rev. B: Condens. Matter Mater. Phys.* **1990**, *42* (9), 5459−5468.

DOI: 10.1021/acssuschemeng.8b05060
ACS Sustainable Chem. Eng. 2019, 7, 2316−2326

(52) Naftel, S. J.; Sham, T. K.; Yiu, Y. M.; Yates, B. W. Calcium l-edge xanes study of some calcium compounds. *J. Synchrotron Radiat.* **2001**, *8* (2), 255−257.
(53) Fleet, M. E.; Liu, X. Y. Calcium $L_{2,3}$-edge XANES of carbonates, carbonate apatite, and oldhamite (CAS). *Am. Mineral.* **2009**, *94* (8−9), 1235−1241.
(54) Ko, J. P. Y.; Zhou, X.-T.; Heigl, F.; Regier, T.; Blyth, R.; Sham, T.-K. X-ray absorption near-edge structure (XANES) of calcium $L_{3,2}$ edges of various calcium compounds and X-ray excited optical luminescence (XEOL) studies of luminescent calcium compounds. *AIP Conf. Proc.* **2007**, *13* (882), 538−540.
(55) Geng, G.; Li, J.; Yu, Y.-S.; Shapiro, D. A.; Kilcoyne, D. A.; Monteiro, P. J. Nanometer-resolved spectroscopic study reveals the conversion mechanism of $CaO\cdot Al_2O_3\cdot 10H_2O$ to $2CaO\cdot Al_2O_3\cdot 8H_2O$ and $3CaO\cdot Al_2O_3\cdot 6H_2O$ at an elevated temperature. *Cryst. Growth Des.* **2017**, *17* (8), 4246−4253.
(56) Mumme, W.; Hill, R.; Bushnell-Wye, G.; Segnit, E. Rietveld crystal structure refinements, crystal chemistry and calculated powder diffraction data for the polymorphs of dicalcium silicate and related phases. *Neues Jahrb. Mineral., Abh.* **1995**, *169* (1), 35−68.
(57) Merlino, S.; Bonaccorsi, E.; Armbruster, T. The real structure of tobermorite 11 angstrom: Normal and anomalous forms, od character and polytypic modifications. *Eur. J. Mineral.* **2001**, *13* (3), 577−590.
(58) Biagioni, C.; Merlino, S.; Bonaccorsi, E. The tobermorite supergroup: A new nomenclature. *Mineral. Mag.* **2015**, *79* (2), 485−495.
(59) Skinner, L. B.; Chae, S. R.; Benmore, C. J.; Wenk, H. R.; Monteiro, P. J. M. Nanostructure of calcium silicate hydrates in cements. *Phys. Rev. Lett.* **2010**, *104* (19), 195502.
(60) Taylor, H. F. W.; Newbury, D. E. Calcium hydroxide distribution and calcium silicate hydrate composition in tricalcium silicate and beta-dicalcium silicate pastes. *Cem. Concr. Res.* **1984**, *14* (1), 93−98.
(61) Bae, S.; Taylor, R.; Hernandez-Cruz, D.; Yoon, S.; Kilcoyne, D.; Monteiro, P. J. M. Soft X-ray spectromicroscopic investigation of synthetic C-S-H and C_3S hydration products. *J. Am. Ceram. Soc.* **2015**, *98* (9), 2914−2920.
(62) Kirkpatrick, R. J.; Brown, G. E.; Xu, N.; Cong, X. D. Ca X-ray absorption spectroscopy of C-S-H and some model compounds. *Adv. Cem. Res.* **1997**, *9* (33), 31−36.
(63) Gartner, E.; Maruyama, I.; Chen, J. A new model for the csh phase formed during the hydration of portland cements. *Cem. Concr. Res.* **2017**, *97*, 95−106.
(64) Li, D.; Bancroft, G. M.; Fleet, M. E.; Feng, X. H. Silicon k-edge xanes spectra of silicate minerals. *Phys. Chem. Miner.* **1995**, *22* (2), 115−122.
(65) Fleet, M. E.; Muthupari, S.; Kasrai, M.; Prabakar, S. Sixfold coordinated si in alkali and alkali-CaO silicophosphate glasses by Si K-edge xanes spectroscopy. *J. Non-Cryst. Solids* **1997**, *220* (1), 85−92.
(66) Li, D.; Bancroft, G. M.; Kasrai, M.; Fleet, M. E.; Secco, R. A.; Feng, X. H.; Tan, K. H.; Yang, B. X. X-ray-absorption spectroscopy of silicon dioxide (SiO_2) polymorphs - the structural characterization of opal. *Am. Mineral.* **1994**, *79* (7−8), 622−632.
(67) Cabaret, D.; Le Grand, M.; Ramos, A.; Flank, A. M.; Rossano, S.; Galoisy, L.; Calas, G.; Ghaleb, D. Medium range structure of borosilicate glasses from Si K-edge xanes: A combined approach based on multiple scattering and molecular dynamics calculations. *J. Non-Cryst. Solids* **2001**, *289* (1−3), 1−8.
(68) Geng, G.; Taylor, R.; Bae, S.; Hernandez-Cruz, D.; Kilcoyne, D. A.; Emwas, A. H.; Monteiro, P. J. M. Atomic and nano-scale characterization of a 50-year-old hydrated C_3S paste. *Cem. Concr. Res.* **2015**, *77*, 36−46.
(69) Soyer-Uzun, S.; Chae, S. R.; Benmore, C. J.; Wenk, H. R.; Monteiro, P. J. M. Compositional evolution of calcium silicate hydrate (C-S-H) structures by total x-ray scattering. *J. Am. Ceram. Soc.* **2012**, *95* (2), 793−798.
(70) Calas, G.; Brown, G. E.; Waychunas, G. A.; Petiau, J. X-ray absorption spectroscopic studies of silicate-glasses and minerals. *Phys. Chem. Miner.* **1987**, *15* (1), 19−29.
(71) Nicoleau, L.; Bertolim, M. A. Analytical model for the alite (C_3S) dissolution topography. *J. Am. Ceram. Soc.* **2016**, *99* (3), 773−786.
(72) Durgun, E.; Manzano, H.; Pellenq, R. J. M.; Grossman, J. C. Understanding and controlling the reactivity of the calcium silicate phases from first principles. *Chem. Mater.* **2012**, *24* (7), 1262−1267.
(73) Henderson, G. S. A Si K-edge EXAFS/XANES study of sodium-silicate glasses. *J. Non-Cryst. Solids* **1995**, *183* (1−2), 43−50.
(74) Gursel, A. P.; Maryman, H.; Ostertag, C. A life-cycle approach to environmental, mechanical, and durability properties of ″green″ concrete mixes with rice husk ash. *J. Cleaner Prod.* **2016**, *112*, 823−836.
(75) Ishida, H.; Okada, Y.; Mitsuda, T. Highly reactive β-dicalcium silicate: II, hydration behavior at 25 °C followed by ^{29}Si nuclear magnetic resonance. *J. Am. Ceram. Soc.* **1992**, *75* (2), 359−363.
(76) L'Hopital, E.; Lothenbach, B.; Scrivener, K.; Kulik, D. A. Alkali uptake in calcium alumina silicate hydrate (C-A-S-H). *Cem. Concr. Res.* **2016**, *85*, 122−136.
(77) Bae, S.; Taylor, R.; Shapiro, D.; Denes, P.; Joseph, J.; Celestre, R.; Marchesini, S.; Padmore, H.; Tyliszczak, T.; Warwick, T.; et al. Soft X-ray ptychographic imaging and morphological quantification of calcium silicate hydrates (C-S-H). *J. Am. Ceram. Soc.* **2015**, *98* (12), 4090−4095.
(78) Ludwig, H.-M.; Zhang, W. Research review of cement clinker chemistry. *Cem. Concr. Res.* **2015**, *78*, 24−37.
(79) Richardson, I. G. The calcium silicate hydrates. *Cem. Concr. Res.* **2008**, *38* (2), 137−158.

DOI: 10.1021/acssuschemeng.8b05060
ACS Sustainable Chem. Eng. 2019, 7, 2316−2326